Cell Reports, Volume *38*

Supplemental information

Identification of the nucleotide-free state as a therapeutic vulnerability for inhibition of selected oncogenic RAS mutants

Imran Khan, Akiko Koide, Mariyam Zuberi, Gayatri Ketavarapu, Eric Denbaum, Kai Wen Teng, J. Matthew Rhett, Russell Spencer-Smith, G. Aaron Hobbs, Ernest Ramsay Camp, Shohei Koide, and John P. O'Bryan

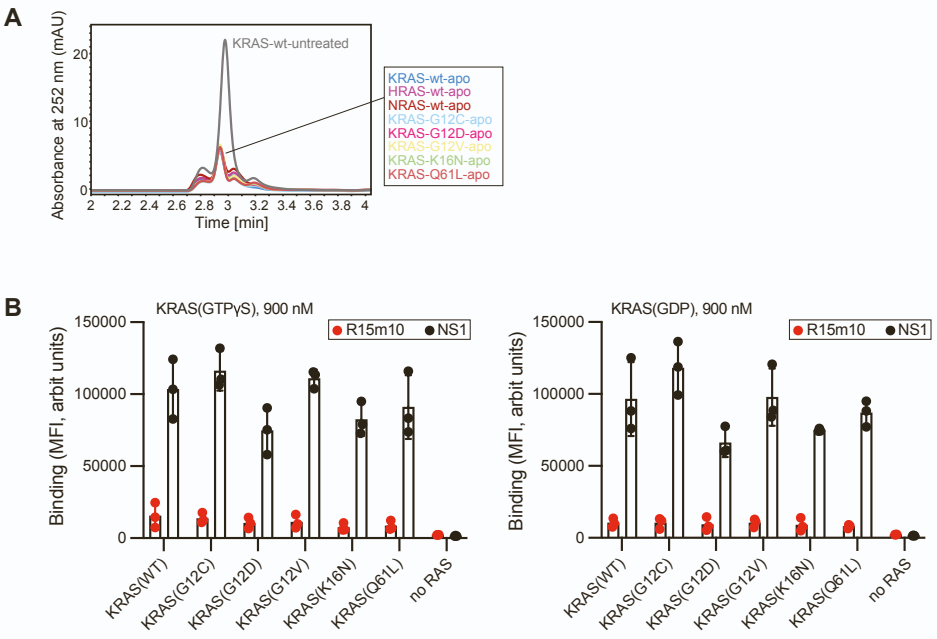

Figure S1. Analysis of apo RAS proteins and binding characterization of R15m10 Monobody, Related to Fig. 1. A. HPLC analysis of nucleotides released from apo mutant RAS protein samples. Each chromatogram represents data from 25 µl of 7 µM sample. **B**. Binding of R15m^{10} to GTPγS- and GDP-loaded states of the indicated KRAS mutants as tested using yeast surface display. NS1, which is nucleotide-state agnostic, is included as a positive control.

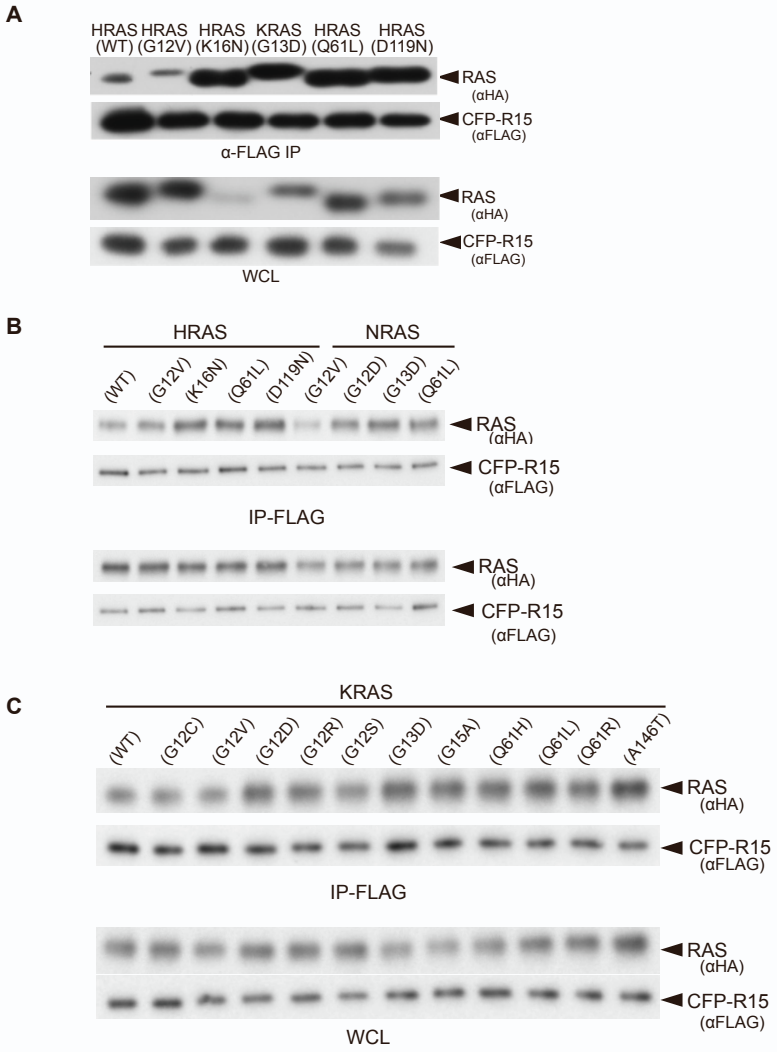

Figure S2. Apo-specific R15 Monobody selectively binds to RAS mutants in cells, Related to Fig. 2. A. Selected RAS mutant proteins were co-immunoprecipitated with FLAG-tagged CFP-R15 Monobody from HEK293T cell lysates. Bottom two panels, expression of HA-tagged RAS proteins and FLAG-tagged CFP Monobodies in whole cell lysates (WCL). IP, immunoprecipitation. **B&C.** Immunoprecipitation and Western blot analysis of R15m^{10} interaction with various oncogenic mutant RAS proteins; HRAS & NRAS (B), KRAS(C). Results were repeated a total of 3 times from independent transfections and quantification of results presented in Figure 2B.

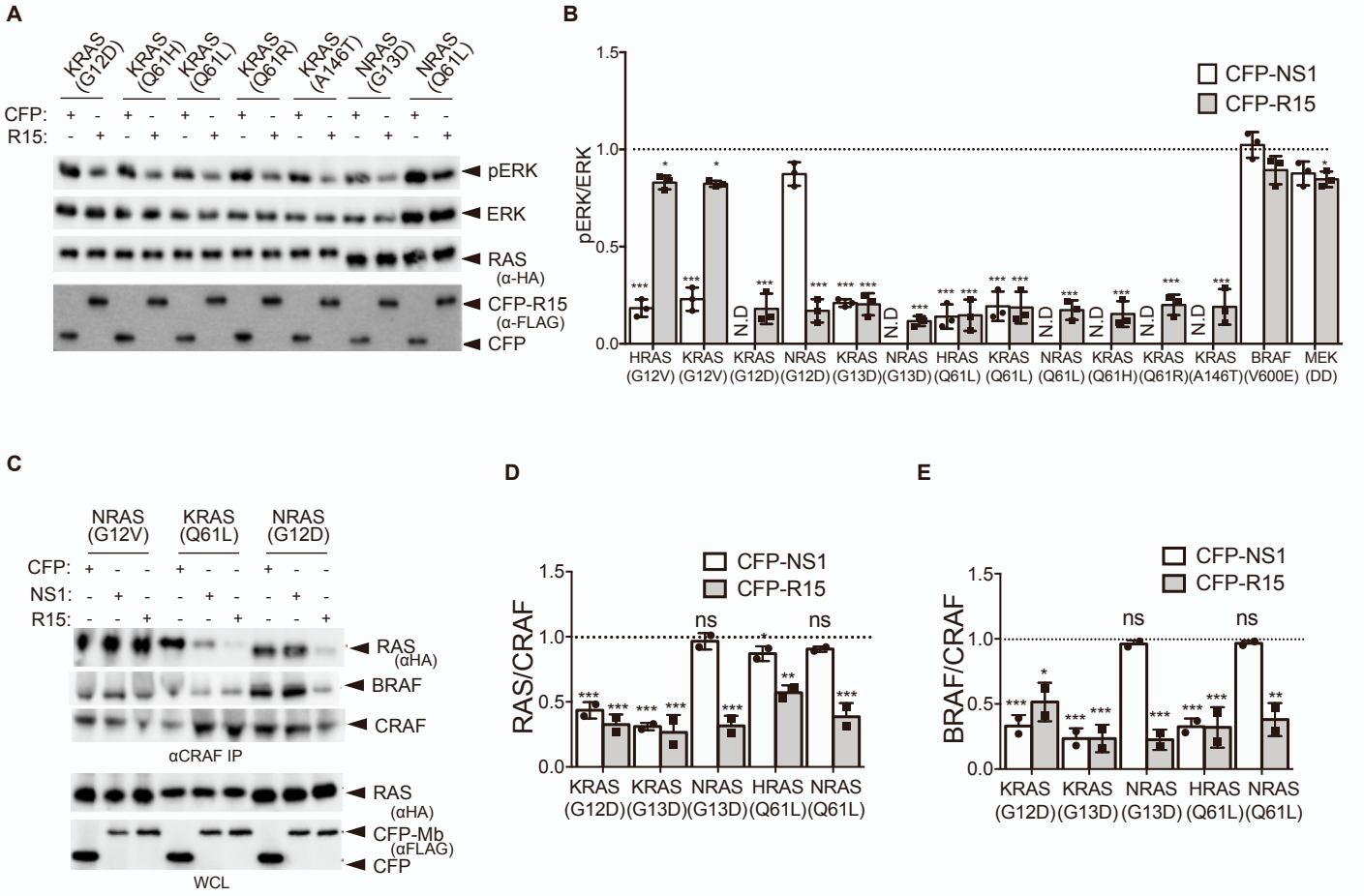

Figure S3. Analysis of R15 effects on ERK-MAPK activation by various oncogenic RAS mutants, Related to Fig. 5. **A**. ERK-MAPK activation was performed as described in Figure 5A and B. **B**. Quantification of ERK-MAPK activation. The results represent the average of three independent experiments +/-s.d. **C**. Effects of R15 on RAS-CRAF association and CRAF-BRAF dimers as described in Figure 5D. **D.** The quantification of R15 effects on RAS-CRAF association and CRAF-BRAF heterodimers. The results represent the average of two independent experiments +/-s.d.

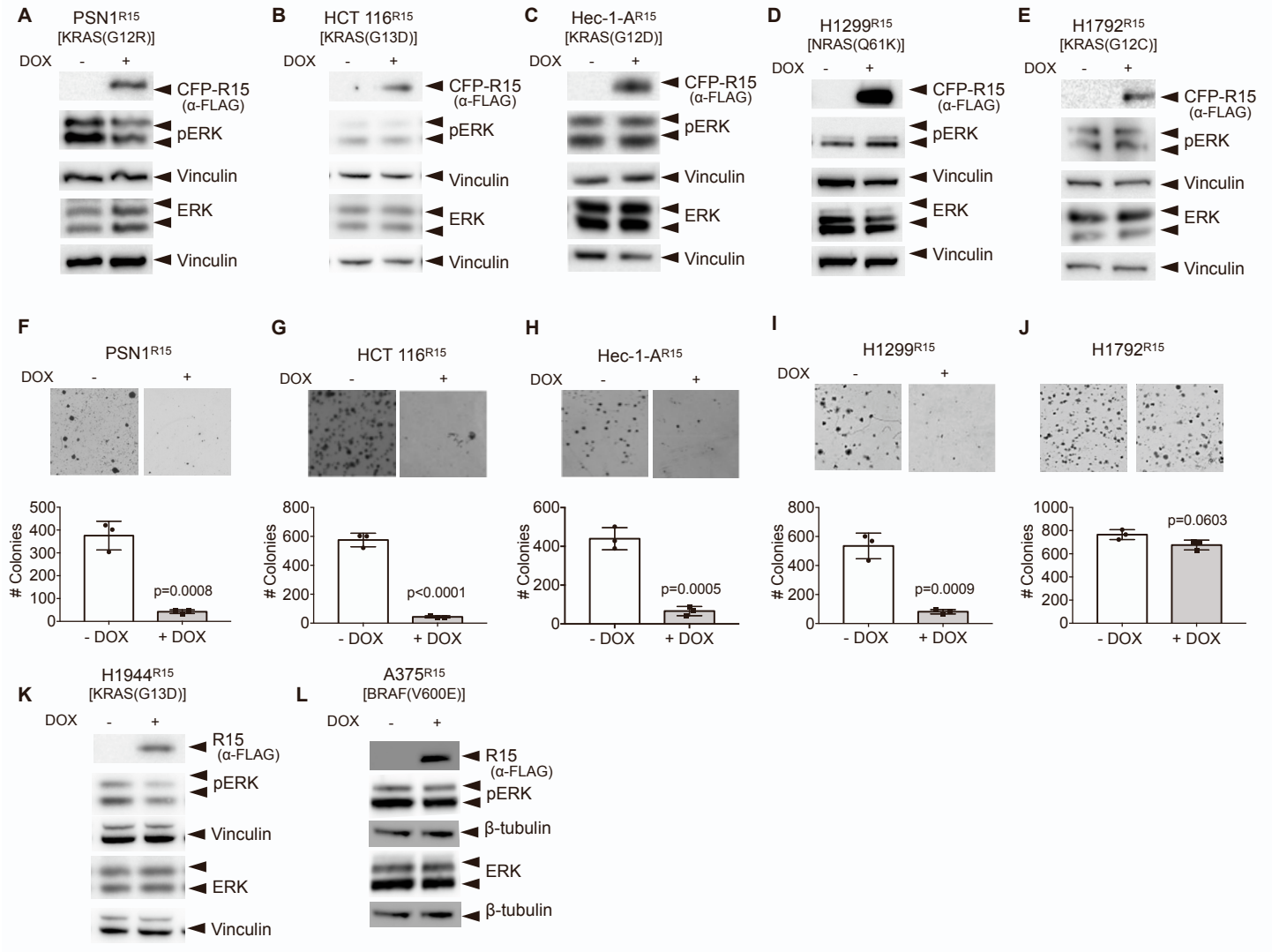

Figure S4. Effect of R15 expression on additional human tumor lines, Related to Fig. 6. A-E. Effect of R15 induction on ERK activation (A-E, K & L) and anchorage independent growth (F-J). Experiments were performed as described in Figure. 6. **A, F.** PSN1^{R15}; **B, G.** HCT116^{R15}; **C, H.** Hec1A^{R15}; **D, I.** H1299^{R15}; **E, J.** H1792^{R15}; K. H1944^{R15}; L. A375^{R15}.

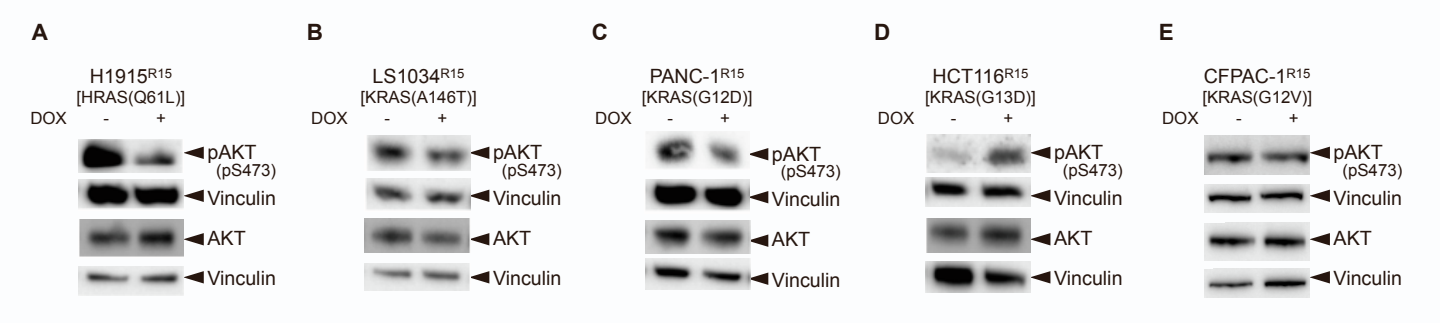

Figure S5. Effect of R15 expression on AKT activation in human tumor cells, Related to Figs. 6 and S4. Experiments were performed as in Figure 6A-E except Western blots were probed for $pAKT^{S473}$ levels.

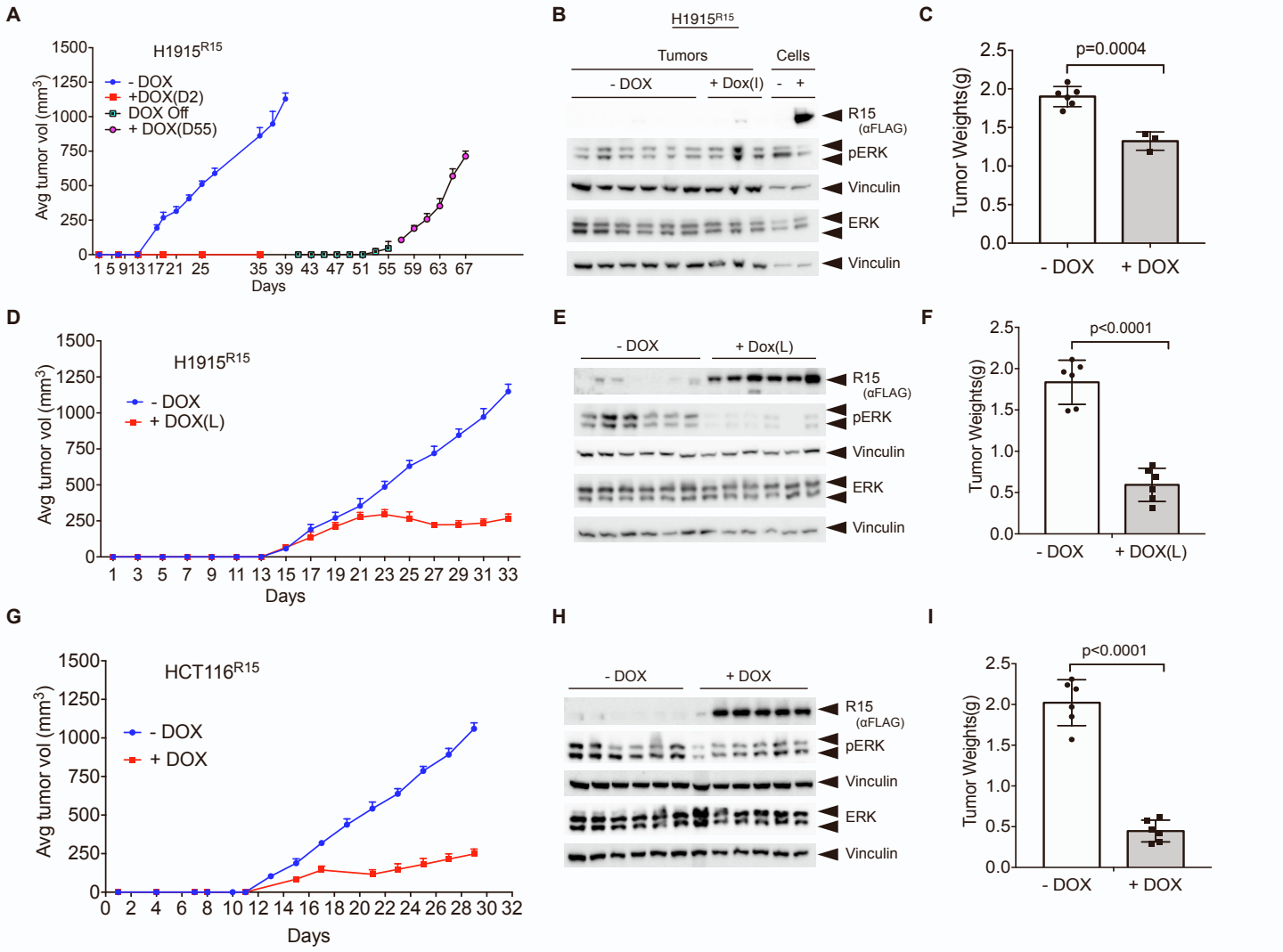

Figure S6. R15 inhibits RAS-driven tumor development in additional cancer lines, Related to Figs. 6 and 7. A-F. $H1915^{R15}$ cells or **G-I.** $HCT116^{R15}$ cells were injected into the flanks of athymic nude mice as described in Figure 7. **A.** Mice were treated with DOX (+) on the day following cell injection or left untreated (-DOX) or +DOX(D2). On Day 41, mice were removed from DOX treatment (DOX off). On Day 55, three mice that exhibited detectable tumors were placed on DOX [DOX(D55)] and tumor growth monitored for an additional 12 days. **B.** Lysates from tumors of untreated mice (Day 39, n=6) and DOX-treated animals (n=3) were analyzed for pERK levels by Western blot as described in Figure 7. The two lanes on the far right represent lysates from parental $H1915^{R15}$ cells grown in culture and treated +/-DOX. **C**. Average tumor weights at experimental end point. **D**. Same as in A except mice did not received DOX until tumors reached a volume of 50-70 mm^3 DOX(L)). **E**. Western blot analysis of tumor lysates as described in Figure 7. **F.** Average tumor weights at experimental end point of $H1915^{R15}$DOX(L). **G**. Mice were treated with DOX (+) on the day following cell injection or left untreated and then monitored for tumor development. Average tumor volume (n=6 per condition) **H. T**umor lysates were analyzed for pERK levels as in B,E. **I**. Average tumor weights at experimental end point of $HCT116^{R15}$.

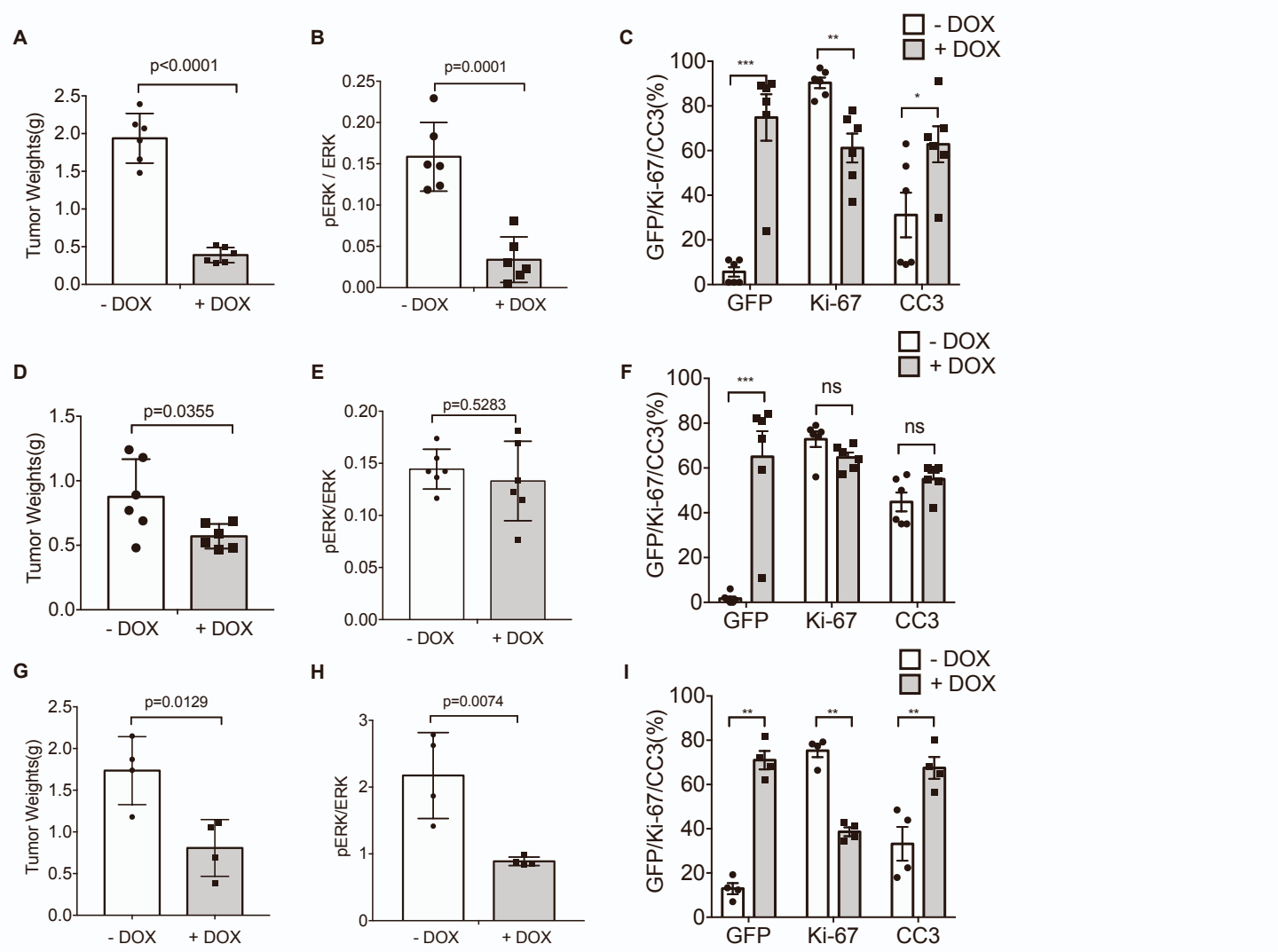

Figure S7. R15 selectively inhibits tumors by decreasing proliferation and inducing apoptosis, Related to Figs. 6 and 7. Effects of DOX induced R15 expression on tumor weights in PDAC xenografts and CRC PDXs. PANC-1(A), CFPAC-1 (D) and huRC/MRC30 (G). Quantification of MAPK signaling from tumor lysates of PANC-1 (B), CFPAC-1 (E) and huRC/MRC30 (H). Tumors from PANC-1^{R15} and CFPAC-1^{R15} PDACs and huRC/MRC30^{R15} were phenotyped by immunohistochemistry for R15(GFP), Ki-67 and cleaved Caspase-3(CC3). **C.** Proportion of Ki-67, and CC3 cells for untreated and +DOX mice in KRAS(G12D) mutant PDACs. **F.** Same as in **C** in KRAS(G12V) mutant PDACs. **I**. Same as in C, F for KRAS(G12D) colorectal PDX.

Cell Line	Origin	Mutation
NCI-H1915	NSCLC	HRAS(Q61L)
LS1034	CRC	KRAS(A146T)
HuP-T3	PDAC	KRAS(G12R)
PANC-1	PDAC	KRAS(G12D)
CFPAC-1	PDAC	KRAS(G12V)
PSN-1	PDAC	KRAS(G12R)
HCT 116	CRC	KRAS(G13D)
Hec-1-A	EAC	KRAS(G12D)
NCI-H1299	NSCLC	NRAS(Q61K)
NCI-H1792	LAC	KRAS(G12C)
NCI-H1944	NSCLC	KRAS(G13D)
A375	MM	BRAF(V600E)

NSCLC: Non small cell lung carcinoma
CRC: Colorectal carcinoma
PDAC: Pancreatic ductal adenocarcinoma
EAC: Endometrial adenocarcinoma
LAC: Lung adenocarcinoma
MM: Metastatic Melanoma

Table S1. Description of the origin and mutation status of various human tumor cell lines. Related to Figs. 6, 7, S5-S7.